ROYAL SOCIETY
OF CHEMISTRY

Check for updates

Photoinduced functionalization of graphene with photocleavable coatings

Elsa Korhonen, [ID] Erich See, [ID] Aleksei Emelianov, [ID] Aku Lampinen, [ID] Maija Nissinen [ID]* and Mika Pettersson [ID]*

Spatially selective functionalization of graphene has gained interest in recent years due to its ability to create more complex and, at the same time, more controllable materials with added functionalities. Photocleavable protecting groups (PPGs) enable the creation of chemically modified areas on material surfaces by releasing the protected molecules upon exposure to light. In this study, graphene coated with photocleavable boron dipyrromethene (BODIPY) derivatives *via* non-covalent interactions was patterned with green laser radiation to create amine-functionalized regions on graphene. The tunability of patterning by changing the irradiation time, laser spot size, or anchor group used to attach on graphene was studied. In addition, the topology and thickness of the photocleavable coatings were investigated. Using BODIPY bearing a pyrene anchor, the patterns created on graphene were more precise than with the naphthalene anchor. The photocleavage-created patterns were visible by both atomic force microscopy and Raman mapping. The presented method demonstrates the high potential of non-covalently attached photocleavable coatings for photoinduced, selective functionalization of graphene.

Introduction

The best-known one-atom-thick material, graphene, has excellent optical, electrical and mechanical properties.[1,2] These properties can be modified, for example, by chemical functionalization. While graphene is a very promising material for many applications, it has relatively poor chemical reactivity and affinity towards biomolecules.[1] For that reason, altering the properties of graphene is a field of extensive research. A convenient way to modify graphene properties is *via* surface functionalization, which involves the addition of functional groups or molecules to the graphene surface. Covalent functionalization is often limited due to the poor reactivity of pristine graphene.[1] However, the utilization of molecules capable of binding through non-covalent interactions expands the possibilities for functionalization and reduces unintended alterations to the graphene properties, which can be caused by covalent functionalization. For this purpose, polycyclic aromatic hydrocarbons, especially pyrene,[3–10] have been widely used as an anchor group on graphene surfaces. Other aromatic anchors used include, for example, naphthalene,[4] anthracene,[11] coronene,[12] and perylene.[13]

The orientation of pyrene on the graphene surface is affected by the concentration. For example, Zhang *et al.*[14] demonstrated that when concentrated solutions of pyrene butyric acid (0.01–1 M) are

Nanoscience Center, Department of Chemistry, University of Jyväskylä, Finland P.O. Box 35, FI-40014 JYU, Finland. E-mail: maija.nissinen@jyu.fi, mika.j.pettersson@jyu.fi

used, the pyrene rings interact through edge-to-face π-stacking with graphene. Additionally, Mann *et al.*[4,5] showed that with low concentrations around 1 μM, molecules bearing a pyrene anchor were more likely to lay flat on graphene, indicating face-to-face π-stacking between a pyrene anchor and graphene. However, the exact conditions required for different stacking modes depend on many factors beyond simple concentration.

Graphene is highly sensitive to species bound to it or in contact with its surface—even unintentional contamination can significantly alter its properties and behavior.[15,16] Because of this, the selective functionalization of specific areas on the graphene surface is also of great interest, especially without the use of covalent bonds. This allows for tailoring certain regions of the graphene surface to have different wetting properties, interact differently with specific biomolecules (for example, to build a multi-channel biosensor), or create chemically differentiated pathways to influence cell growth. Existing non-selective functionalization techniques either functionalize the entire graphene surface or randomly alter areas in an uncontrolled fashion.[1] Currently, only a handful of techniques allow for the selective alteration of the graphene surface, such as those utilizing oxidation,[17–19] directed functionalization,[20,21] targeted metallization,[22] direct writing with grafting ink,[23] mask-based lithography,[24,25] and the use of templates.[26] Methods utilizing photocleavage of surface-bound molecules are studied even less. Hirsch *et al.* have introduced covalent patterning of graphene by utilizing the photolysis of dibenzoyl peroxide,[20] silver trifluoroacetate,[27] and 1-fluoro-3,3-dimethylbenziodoxole.[28]

Photoprotecting groups (PPGs)[29] offer an alternative method for spatially selective graphene functionalization. They allow the release of the protected functional groups (*i.e.* cargo) *in situ via* photoexposure in specified regions. Visible light-sensitive PPGs offer a less damaging option for biological and medical applications compared to more conventional UV-light-sensitive PPGs.[30] *meso*-Methyl EtBODIPY PPG is a rare example of an amine releasing green light-sensitive PPG.[31] Photoprotection of amines is especially useful for biological and medical applications, since amines are biologically relevant functional groups that can be found in, for example, neurotransmitters and amino acids.

Previously, our group introduced a photocleavable BODIPY derivative (**1**; Scheme 1) that binds non-covalently to graphene through a phenyl anchor group and cleaves upon irradiation with green light both in solution and on graphene.[32] In addition, we demonstrated the spatial selectivity of the photolysis. Recently, we reported the synthesis, characterization and photophysical properties of two other BODIPY derivatives with extended aromatic terminal groups, naphthalene (compound **2**) and pyrene (compound **3**), to enhance non-covalent π–π stacking on a pristine graphene substrate.[33] It was observed that compounds **1** and **2** have similar photophysical properties, whereas compound **3** had significantly lower fluorescence quantum yield, was capable of intramolecular energy transfer, and, in the solid state, its crystal packing was governed by π-interactions between pyrene units. The photocleavage studies in solution showed that compounds **1** and **2** had a faster photocleavage rate than compound **3**. In an oxygen atmosphere, the photocleaved

BODIPY core decomposes fully *via* secondary reactions, while in inert conditions, photocleavage was faster, and the BODIPY core did not decompose further for any of the compounds **1–3**. We expect that when attached to graphene, the compounds follow the same photocleavage routes through the photo-S_N1 mechanism as in solution,[34] but the photodecomposition pathway of the BODIPY core may vary (Scheme 1).

Here, we functionalize graphene non-covalently with two BODIPY derivatives **2** and **3** and demonstrate the writing of linear patterns on their coatings on graphene by irradiation with a green laser. We also studied the tunability of patterning by changing the anchor group binding to the graphene surface, irradiation time and laser spot size. In addition, we studied the surface topology of graphene with photocleavable coatings and determined the thickness of the self-assembled photocleavable layers. This work demonstrates that non-covalently attached photocleavable coatings can be patterned using a laser, and the size of the patterns or the degree of photocleavage can be controlled.

Methods

Graphene deposition

Graphene was synthesized by chemical vapor deposition (CVD) and transferred onto silicon/silicondioxide (Si/SiO$_2$) substrates with metal grids according to a previously reported procedure.[32] Compounds **2** and **3** were synthesized as described in our previous work.[33]

To enhance the deposition and formation of a self-assembled layer on the graphene substrate, the highest feasible concentrations of the BODIPY compounds in alcohol solutions were used: a 1 mM solution of compound **2** in ethanol (AA, Altia Oyj) and a 0.06 mM solution of compound **3** in 1-butanol (>99.5%, VWR). The deposition of all compounds was performed by placing a few droplets of the corresponding solution on the graphene-on-Si/SiO$_2$ substrate, which was sealed in a small glass enclosure to prevent evaporation and left in the dark for 1 h. Afterwards, the samples with compound **2** were rinsed twice with ethanol, once with isopropanol (>99.8%, VWR), and then gently blown dry with a N$_2$ flow. Samples with compound **3** were rinsed first with 1-butanol, then with ethanol, and finally with isopropanol, and then gently dried with a N$_2$ flow. The rinsing step was done to remove any unbound photocleavable compounds.

Determination of the thickness of the photocleavable layer (scratch test)

AFM measurements were taken using a Bruker Icon AFM in off-resonance PeakForce Tapping® mode with Bruker ScanAsyst-Air tips. A scratch test was performed using tweezers to gently scratch the pristine graphene surface, allowing for the measurement of the height difference between the Si/SiO$_2$ substrate and the graphene using AFM. After this, the graphene was covered with each BODIPY derivative (**2** and **3**) separately, and another AFM scan was performed on the same sample after another scratch. To measure the height, five profiles covering graphene
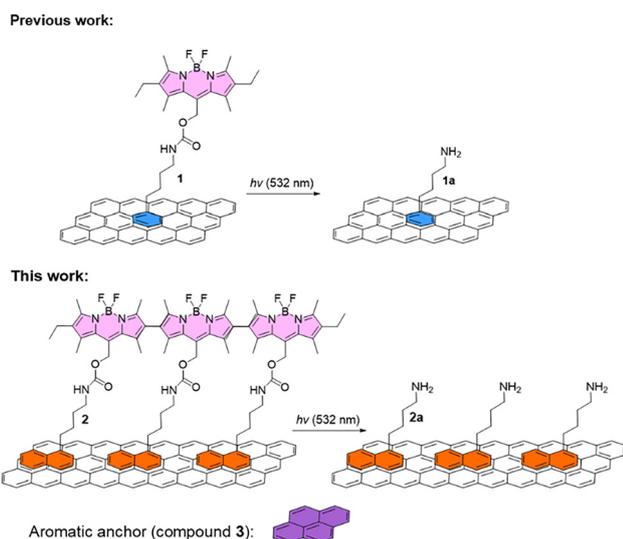
Scheme 1 Schematic presentation of non-covalent binding of BODIPY derivatives on graphene through π-stacking and outcome after irradiation with green light. The BODIPY core is marked in pink, and the anchor groups are presented in different colors. Previous work: localized photocleavage of BODIPY derivative **1** with phenyl as anchor group (blue), releasing amine **1a** upon green light exposure. This work: linear patterning of graphene coated with BODIPY derivatives **2** with naphthalene (orange) or **3** with pyrene (purple) anchors, releasing the corresponding amines as the desired patterns.

This journal is © the Owner Societies 2025

Phys. Chem. Chem. Phys., 2025, **27**, 22508–22519 | **22509**

and SiO$_2$ areas at the edge of each scratch, both before and after BODIPY deposition, were plotted, and the heights were calculated based on average values. To measure the roughness, sections of the substrate that were relatively free of debris/defects were selected, and the area measurements of R_a (average roughness) and R_q (root mean square roughness) were extracted from the data using the Gwyddion data analysis program.

AFM measurements of the patterns

The areas patterned with the laser were measured with the same AFM equipment. Relative height comparisons were performed using the Step analysis tool of Nanoscope Analysis 1.9 (Bruker) to show height differences between irradiated and non-irradiated areas of compounds **2** and **3** on graphene. The tool takes several cross-sectional profiles parallel to each other and averages them to enable measurements of the average height difference.

Raman measurements

Single-spot measurements were taken using a DXR Raman Microscope (Thermo Scientific) with a 532 nm excitation laser. The laser wavelength was selected to be within the compound's photocleavage range, ensuring that the cleavage and measurement spots were exactly the same size. Using the 10× objective, the power was set to 10 mW, and the individual spot irradiation time was 5 s. After this initial irradiation, Raman spectra were measured after 5, 50, 100, 250, 500, and 1000 s of further laser exposure at the same power level as the photolysis.

To create linear patterns on the surface of the samples, the mapping function of the OMNIC Raman spectroscopy program with a 532 nm laser was utilized. The spot sizes for the 10× and 50× objectives were 2.5 and 1.5 μm, respectively. For 10×, a power of 10 mW was chosen, identical to the power used for the single-spot Raman measurement and cleavage. The power selected for the exposure with the 50× objective was 1.2 mW, chosen so that when the reduced spot size was taken into account, the overall irradiation dose was similar to that for the 10× objective. A step size of 2 μm was chosen for the 10× objective patterning to ensure that the irradiation spots partially overlapped with each other. For 50×, the minimum available step size of 1 μm was selected due to the limitations of the stage and software. Irradiation time for each sample to create linear patterns was 45 s per spot.

Raman maps of the samples with linear patterns were imaged using the same mapping function of the Raman microscope described above for line patterning, but instead of lines, a rectangular area was defined. Laser power was set to 10 and 1.2 mW, and the step sizes of 2 μm and 1 μm were used for measurements with the 10× and 50× objectives, respectively. Scan times were set to 2 s to prevent further cleaving during the scan.

Results and discussion

Characterization of photocleavable coatings

BODIPY compounds with varying anchor groups had different morphologies on graphene. AFM measurements of compound

1 (1 mM in ethanol) on graphene before and after irradiation were inconclusive, so it was not studied further. For compound **2**, the AFM image revealed a nonuniform dispersion of the material in randomly shaped areas with a typical height between 0.5–1.1 nm (Fig. 1(b) and (d)). For compound **3**, the material is also nonuniformly distributed, but it occurs in small particle-like areas with a typical height between 0.48–1.3 nm (Fig. 1(f) and (h)).
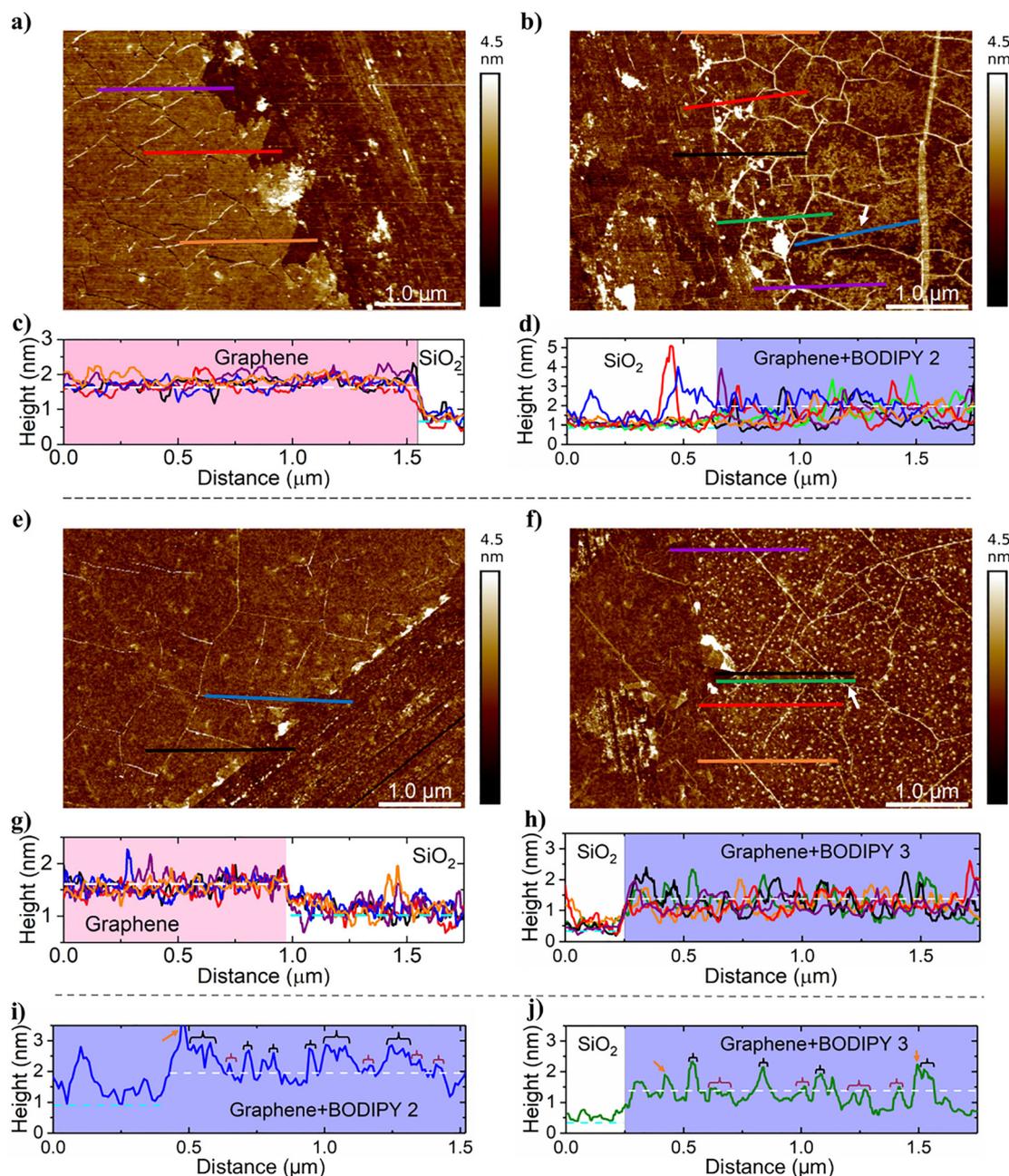
A scratch test was done to determine the thickness of each photocleavable layer. Based on the scratch tests, the average height differences for each self-assembled layer on top of the graphene were 0.24 nm for compound **2** (naphthalene anchor) and 0.48 nm for compound **3** (pyrene anchor), measured from height sensor images (Fig. 1, Table 1, and Tables S1, S2). The greater average height of compound **3** is due to substantial particle formation (Fig. 1(f) and (h)). The R_q (root mean square roughness) and R_a (average roughness) increased when the graphene was coated with photocleavable compounds.

Representative height profiles of each photocleavable layer are shown in Fig. 1(i) and (j). The observed heights for compound **3** indicate the presence of a monolayer (0.48 nm, Fig. 1(j); purple brackets) and a double layer or different conformation (1.3 nm, Fig. 1(j); black brackets). For compound **2**, height profiles taken across the scratch do not result in a reliable value of the height of the coating because the baseline is on the same level on both sides of the scratch. The transition area between the substrate and graphene with BODIPY coating (compound **2**) is irregular, meaning that graphene might be missing or there is graphene left in the scratch. Hence, we took an additional height profile far away from the scratch as shown in Fig. 1(b) and (i) as a blue line. Based on the representative height profile showing areas with heights close to 1.1 nm and 0.5 nm (Fig. 1(i); black and purple brackets, respectively), the same observation about mono and double layers and conformational change was made as for compound **3**. Other high peaks marked with orange arrows in Fig. 1(i) and (j) are from the cracks or folds on the surface.

The heights of compounds **2** and **3** in the crystalline form reported in our previous paper[33] were approximately 0.97 nm and 0.45 nm, respectively (Fig. S1 and S4). These values cannot be directly compared with the molecular dimensions on self-assembled layers, as in the crystalline state, the molecules orient to allow the closest packing with themselves, whereas when self-assembling on a surface, interaction with graphene may change the conformation, and that way change the height of the molecule.

The possible height ranges for compounds **2** and **3** on graphene were estimated by measuring relevant dimensions from their crystal structures (Fig. S1 and S4). The estimated height of compound **2** is 0.32–1.44 nm, assuming a face-to-face stacking interaction between the naphthalene anchor group and graphene and the minimum height to be the minimum distance of π-stacking. The distance of π-stacking between graphene and aromatic rings is typically around 0.322–0.354 nm.[35,36] When the distance of weak interaction is considered, regions of compound **2** with lower height on graphene

22510 | *Phys. Chem. Chem. Phys.*, 2025, **27**, 22508–22519

This journal is © the Owner Societies 2025

Fig. 1 AFM scratch test height measurements before and after coating the graphene with photocleavable compounds. (a) Pristine graphene before and (b) after coating with BODIPY compound **2** (1 mM in ethanol). (c) and (d) correspond to several cross-sectional height profiles (solid lines) from a and b taken across the scratch edge and their averages (dashed lines) showing either the differences between pristine graphene and the scratch or the BODIPY-coated graphene and the scratch. (e) Pristine graphene before and (f) after coating with BODIPY compound **3** (0.06 mM in 1-butanol), with (g) and (h) showing the corresponding height profiles from g and h as described above. Different colors in the height profiles d and h correspond to different line scans shown in the AFM images b and f. (i) One representative line scan from b (blue line marked with white arrow) showing areas related to the coating of compound **2** by black brackets (higher regions) and purple brackets (lower regions). (j) One representative line scan from f (green line marked with white arrow) showing areas related to the coating of compound **3** by purple brackets (lower regions) and black brackets (higher regions). Orange arrows indicate cracks in graphene.

(0.5 nm) indicate that compound **2** is lying on graphene in a planar orientation (Fig. S2). In addition, the maximum height is achieved by changing the molecular geometry compared to the crystal structure. However, the regions with higher values indicate either double layers or a different conformation of compound **2** (Table 1). In double layers, molecules in the upper layer no longer interact with graphene, which changes their conformation compared to those in the layer directly on top of the graphene.

Similarly, the dimensions of compound **3**, while lying horizontally on graphene, were estimated to be 0.32–1.65 nm

This journal is © the Owner Societies 2025

*Phys. Chem. Chem. Phys.*, 2025, **27**, 22508–22519 | **22511**

Table 1 General characterization of pristine graphene surface and with photocleavable coatings of compounds **2** and **3**. Standard deviation is shown for the average heights

Compound	Avg. bare graphene height [nm]	Avg. coated graphene height [nm]	Avg. height difference [nm]	Typical coating height (without graphene height)/estimated max. height (XRD) [nm]	Graphene roughness (R_q/R_a) [nm]	Graphene-with-coating roughness (R_q/R_a) [nm]	Difference in roughness (R_q/R_a) [nm]
2	0.911 ± 0.168	1.150 ± 0.576	0.24	0.5–1.1/1.44	0.352/0.231	0.764/0.582	0.412/0.351
3	0.579 ± 0.139	1.125 ± 0.332	0.48	0.48–1.3/1.65	0.385/0.262	0.584/0.420	0.199/0.158

(Fig. S4). When taking the distance of weak interaction into account, lower regions (Fig. 1(j); 0.48 nm) corresponded well with the crystal structure of compound **3** (Fig. S4 and S5; 0.45 nm), suggesting a similar but more flat orientation on the graphene. In addition, the heights of taller regions (1.3 nm) match well with the conclusion related to the double layer. The orientation of compound **3** directly on graphene is most likely similar to that in the crystal structure (Fig. S5) and in the upper layer, molecules are partly pointing upwards.

Theoretical binding energies for π–π-stacking interaction of benzene, naphthalene and pyrene with graphene are −10.0 kcal mol^{-1},[37] −17.6 kcal mol^{-1},[38] and −26.8 kcal mol^{-1},[39] respectively. Together with our experimental results, they are in agreement with the observation that the phenyl anchor (compound **1**) resulted in less stable coating, whereas the pyrene anchor in compound **3** had a tendency for particle formation, which might be due to the relatively strong π-interactions between the pyrene anchor groups. In addition, our results prove
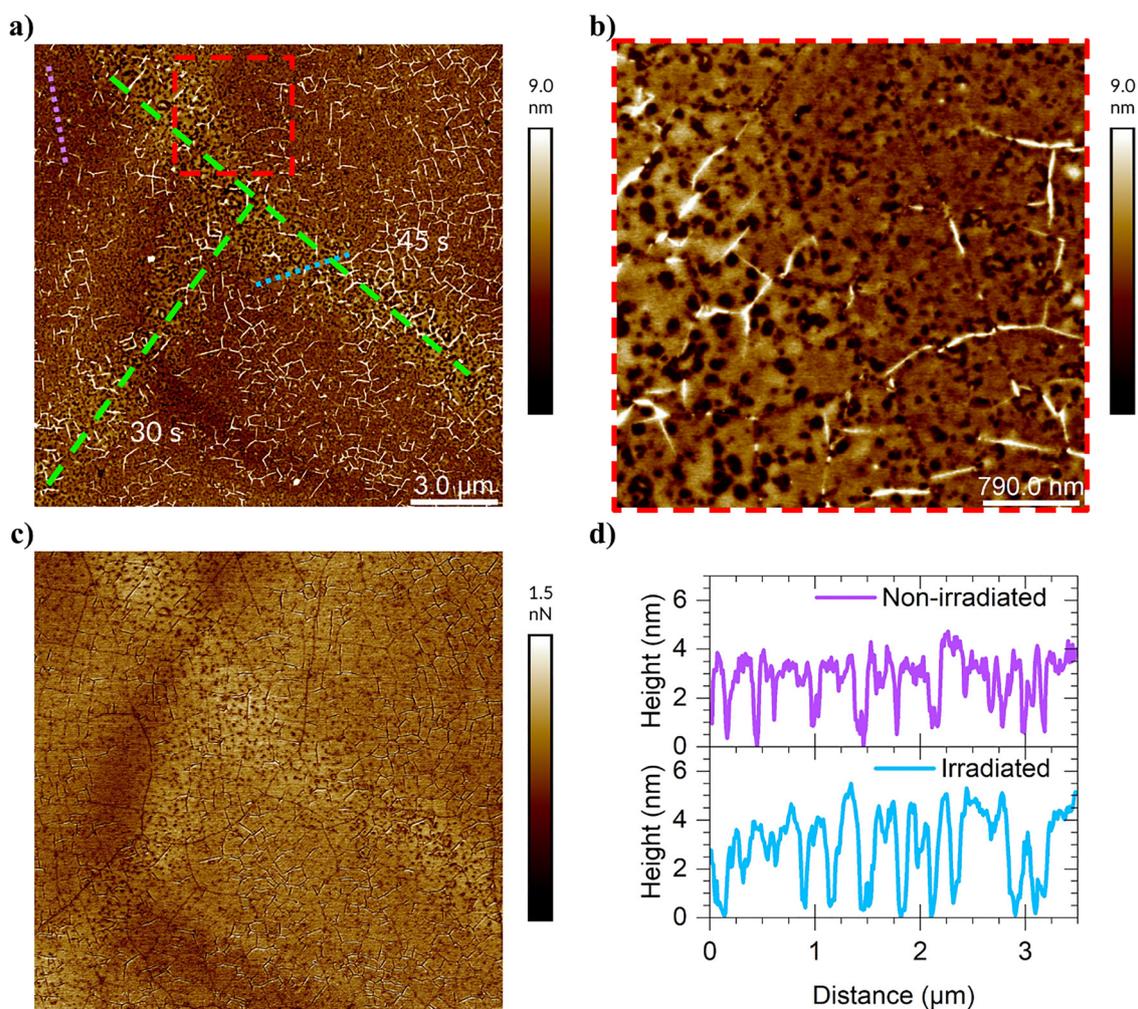
Fig. 2 (a) AFM topography image of pristine graphene covered with compound **2**. The areas highlighted with a green dashed line were irradiated with the green laser (50× objective). The area highlighted with red dashed lines is shown magnified in (b) to highlight the difference in topography between the irradiated (left) and non-irradiated (right) areas. (c) Simultaneously acquired AFM adhesion measurement from the same area, showing the slight difference in adhesion between the irradiated and non-irradiated areas. (d) Cross-sectional profiles taken from (a), which are indicated by dotted lines of the corresponding colors.

22512 | *Phys. Chem. Chem. Phys.*, 2025, **27**, 22508–22519

This journal is © the Owner Societies 2025

that naphthalene as an anchor group binds strongly enough to form a coating.

Surface studies of patterned regions

AFM imaging was used as an additional tool for Raman spectroscopy (described later) to further characterize the photocleavage. Surface patterning of coated graphene was performed with a 532 nm wavelength Raman excitation laser after the deposition of a photocleavable layer. To differentiate between the actual patterning and AFM noise, the patterns in the sample of compound **2** were made to diagonal lines which touch each other: one drawn at a 45 s exposure per spot and the other at a 30 s exposure per spot, both using the 50× objective at 1.2 mW of power and taking 1 μm steps between spots (Fig. 2(a)). Although the chosen exposure time is too short for complete photocleavage (as described in more detail in the Raman section), this exposure time was selected because it is

long enough to be detectable in the system and short enough to be achieved relatively quickly with the existing exposure setup.

A very slight increase in height (1–2 nm, Fig. 2(a), (b) and (d)) and a change in adhesion (Fig. 2(c)) were observed for both exposure lines on the sample with compound **2**, differentiating the exposure lines from the surrounding substrate. Interestingly, there appeared to be a dramatic increase in roughness in the patterned areas of the sample, with R_a of approximately 1.48 nm compared to R_a of 0.75 nm in a similarly sized region in the non-patterned area. Even visually, a clear difference in the surface could be seen at higher magnifications with regard to the topography between patterned and unpatterned regions (Fig. 2(b)). In the patterned area, the holes in the material become wider, and while they reached the same "depth", the area around the rim was higher, making the holes appear 'deeper' (Fig. 2(d)). This matches the perceived gain in height in Fig. 2(a) and could be compatible with agglomeration of **2**
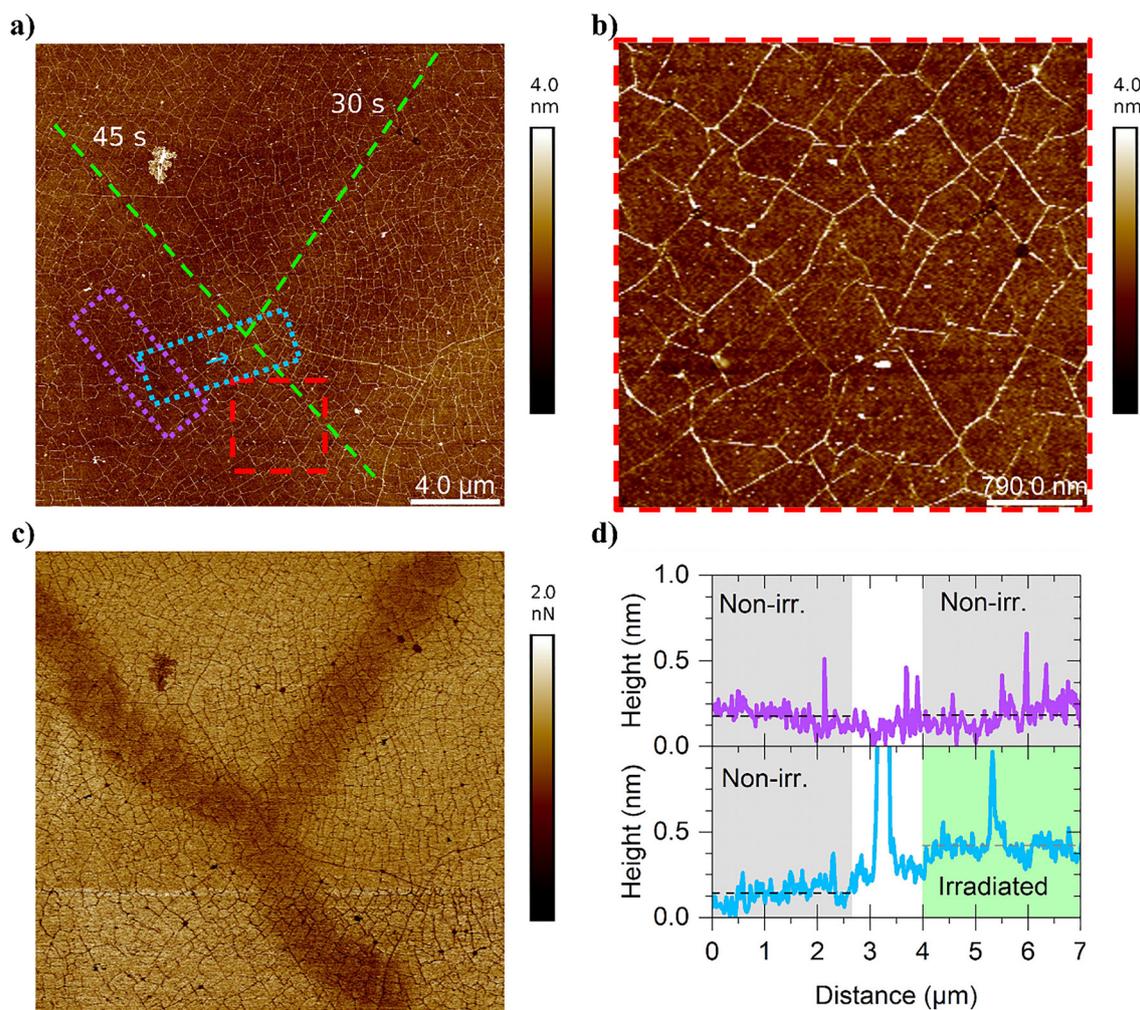
Fig. 3 (a) AFM topography image of pristine graphene covered with compound **3**. The areas highlighted with a green dashed line were irradiated with the green laser (50× objective). The area highlighted with red dashed lines is shown magnified in (b) to highlight the lack of differences in topography between the irradiated (top-right) and non-irradiated (bottom-left) areas. (c) A simultaneously acquired AFM adhesion measurement from the same area showing the clear difference in adhesion between the irradiated and non-irradiated areas. (d) Relative height comparisons between non-irradiated and non-irradiated (top) and non-irradiated and irradiated (bottom) areas. These have been taken from (a) from the areas indicated by dotted lines of the same colors and arrows indicating the direction where the distance increases.

This journal is © the Owner Societies 2025

Phys. Chem. Chem. Phys., 2025, **27**, 22508–22519 | **22513**

after the cleavage and a non-uniform substrate covering. The important outcome of this experiment is that photocleavage is observable by AFM by changes in topography, adhesion, and morphology of the material.

Comparison with the AFM image from the scratch test (Fig. 1(b)) reveals that the surface topologies are different, even though the same sample treatment and concentrations were used. In Fig. 2(b), there seems to be a thicker layer of compound **2** with holes instead of unevenly distributed and randomly shaped areas as in Fig. 1(b). Based on this, there is variation in number of layers forming during the preparation process.

For the sample made with compound **3**, the change in height was more challenging to interpret, as only a slight but still significant increase in the average height (roughly 0.3 nm) was observed (Fig. 3(a) and (d)). However, the change in adhesion was very stark and clear, demonstrating a clear difference between the patterned and unpatterned areas (Fig. 3(c)). Measurements on the patterned and unpatterned areas showed no discernible difference in roughness or appearance of large 'holes'. While the R_a and R_q values varied slightly, the R_a values were all around 0.3 nm, with the significant variations seeming to be more a factor of the graphene sheet than the photocleavage.

Compound **3** formed a clearly smoother coating in the sample used for the photocleavage experiment (Fig. 3(b)) than in the scratch test (Fig. 1(f)). A possible reason might be related to the solubility of compound **3** in 1-butanol, resulting in compound **3** being less soluble in the solution used for sample preparation for the scratch test. Due to the differences in AFM images between the scratch test and the photocleavage experiments, the method could be improved by changing the solvent to better solubilize compound **3** or by trying the immersion method instead of drop casting.

Based on our previous studies, compound **3** exhibits a photocleavage rate that is approximately half that of compound **2** in solution.[33] The same relation may also occur in a dry state, suggesting that smaller changes in layer roughness and height are due to a lower degree of photocleavage of **3**. In addition, the probability for edge-to-face stacking between aromatic anchor groups and graphene (Fig. S3) were ruled out due to the relatively low concentrations used (1 mM for compound **2** and 0.06 mM for compound **3**). Instead, the concentration must be around 1 mM for high-coverage monolayer formation *via* face-to-face stacking interactions on graphene (for pyrene as an anchor group).[8] As discovered by Zhang *et al.*,[14] pyrene butyric acid concentrations must exceed 10 mM for edge-to-face stacking on graphene, suggesting that a higher concentration is required for the naphthalene anchor (**2**).

In both cases, the increase in height with cleavage is sensible. In the standard photoreaction pathway of BODIPY-based PPGs, the caged compound is released through carbamate bond breaking, followed by photodegradation of the BODIPY core to various photodegradation products.[31,40] Consequently, exposed areas may have contained several degradation species since the samples were not rinsed before AFM measurement. Several individual species interacting *via* weak interactions are likely to occupy more space than a compact,

covalently bound structure, similarly to how several Legos™ snapped together in an orderly fashion take up less physical space than if they are taken apart and left in a pile. More rigorously, it is plausible that separate molecular fragments take more space than their covalently bound compound because covalent bonds are much shorter than the sum of the van der Waals radii.

Furthermore, the results provide evidence that we are not simply ablating the film and/or the graphene beneath it when patterning with Raman. This reinforces the data presented in the next section regarding the single-spot Raman measurements (see the chapter on Raman), suggesting that there is no ablation or destruction of the graphene surface.

A change in adhesion also suggests that a chemical change occurred on the surface, further reinforcing that photocleavage has taken place. While the samples with **2** and **3** showed adhesion changes in opposite directions, they were measured on different days with different tips (albeit of the same type). Therefore, as the adhesion measurements were not calibrated, the direction of the difference and absolute values cannot be directly compared. The difference, however, is real. The adhesion data indicate the difference between the patterned and unpatterned areas on the same sample, reinforcing the creation of chemically different regions.

Raman measurements

To confirm the adhesion and photocleavage of compounds **2** and **3** on the graphene substrate, Raman measurements of the samples were taken using the 532 nm laser, allowing both patterning and cleavage at the same spot without moving the sample, thereby ensuring that we were measuring and cleaving the same spot. The normalized Raman spectra measured at 5 s for both samples (**2** and **3**) are roughly similar and agree with our previous results with **1**, showing several resonance Raman peaks of the BODIPY moiety[32] (Fig. 4(a)). This is reasonable since, although the anchoring groups are different, the BODIPY core is the same in all the compounds, and the electronic excitation responsible for the resonance Raman effect is localized to the same moiety in all the compounds.

Many of the peaks in Fig. 4(a), such as those found at 1178 cm^{-1} (A), 1276 cm^{-1} (B), and 1552 cm^{-1} (C), also map well to the resonance Raman spectra for BODIPY dye laid out in Sandoval *et al.*,[41] which looked at the resonance Raman spectrum of a BODIPY molecule attached directly to a single benzene ring. However, there are some exceptions, such as the strong peak at approximately 1225–1226 cm^{-1} (D). This peak appeared in all three photocleavable compounds **1–3** but not in the compound of Sandoval *et al.*[41] Our previous work[32] shows that this peak is highly sensitive to the photodecay process, and this is the case also for compounds **2** and **3** (Fig. 4(b) and (d)), with the peak intensity dropping by over 75% from 5 s to 1000 s of exposure, before taking the loss of fluorescence into account. For comparison, the G-band of graphene (G) is visible at 1600 cm^{-1} in all samples and remains stable under irradiation.

Another area of interest is at 1130–1140 cm^{-1} (E) region, where the peak shifts from 1140 cm^{-1} to 1130 cm^{-1} over the

22514 | *Phys. Chem. Chem. Phys.*, 2025, **27**, 22508–22519

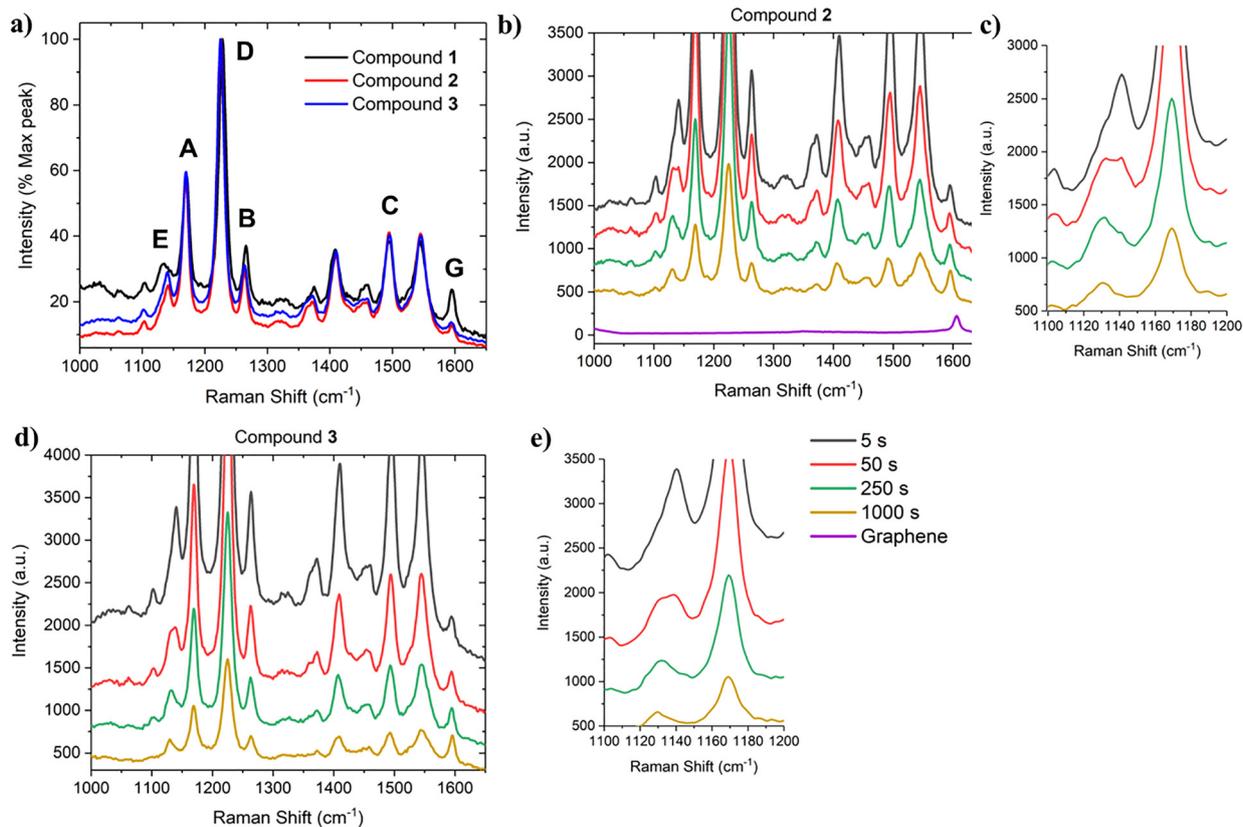This journal is © the Owner Societies 2025

Fig. 4 (a) The Raman spectra of the compounds **1–3** at 5 s (spectrum of **1** is from our previous work[32]). The peaks are labelled as discussed in the text. (b) The resonance Raman spectra of compound **2** at various exposure doses, and (c) zoom in showing the peak decay and shift at $1130-1140$ cm^{-1}. (d) The resonance Raman spectra of compound **3** at various exposure doses, and (e) zoom in showing the peak decay and shift at $1130-1140$ cm^{-1}.

course of the exposure (Fig. 4(c) and (e)). There is a clear spectral change in this region, which could be due to either the appearance of a new peak at 1130 cm^{-1} upon photolysis or two originally overlapping peaks bleaching at different rates. Previous work suggests that the $1130-1140$ cm^{-1} range may be a C–N vibrational mode,[42] so its change and transformation here would be consistent with the carbamate bond breaking during the photocleavage of **2** and **3**, revealing anchors **2a** and **3a** with amino groups (Scheme 1). Therefore, we assign this peak to the C–N stretching vibration, indicative of the carbamate bond.

Comparison of the Raman spectra of compounds **2** and **3** with pristine graphene indicates transfer of electron density from the BODIPY compounds to graphene upon non-covalent binding. The positions of the G- and 2D-bands of graphene coated with the compound **2** are before binding 1606 cm^{-1} and 2695 cm^{-1} (Fig. 4(b) and Fig. S9) and after binding 1595 cm^{-1} and 2686 cm^{-1} (Fig. 4(b)). For compound **3**, the corresponding values are before binding 1602 cm^{-1} and 2690 cm^{-1} (Fig. S9) and after binding 1595 cm^{-1} and 2687 cm^{-1} (Fig. 4(d)). In both cases, both frequencies downshift. The initial values indicate relatively strong hole doping, which is typical for graphene on a SiO$_2$ substrate after transfer with PMMA. After non-covalent binding, the shift of the bands indicates a reduction in hole doping, *i.e.* transfer of electron density from the molecular

compounds to graphene, but overall, graphene still remains hole-doped.[43] The positions of the G- and 2D-bands do not significantly change after irradiation and photocleavage, indicating that the doping doesn't change further.

Raman mapping

Next, we explored the spatial selectivity and resolution of the photocleavage of the deposited compounds. Using the mapping function of the Raman system, we created lines using 45 s doses per spot at 532 nm, then followed up with a short, 2D-map measurement to compare the intensities of the selected peaks. While a 45 s exposure at this power (10 mW for 10× and 1.2 mW for 50×) is not a full exposure, this time point was chosen because it still showed a significant drop in both fluorescence and peak intensity at 1226 cm^{-1} to demonstrate the patterning potential of compounds **2** and **3** without taking overly long to pattern when using the 50× objective. Linear patterns were drawn on the surface using the 10× and 50× objectives with the laser path shown by a dashed yellow line in Fig. 5. The 1226 cm^{-1} line was selected to create the intensity maps based on our previous work[32] and the above resonance Raman, demonstrating a strong correlation with our compounds and their photocleavage.

A cross-section of each Raman map was taken (shown as a red dotted line in Fig. 5(a)–(d)) and plotted to examine the data
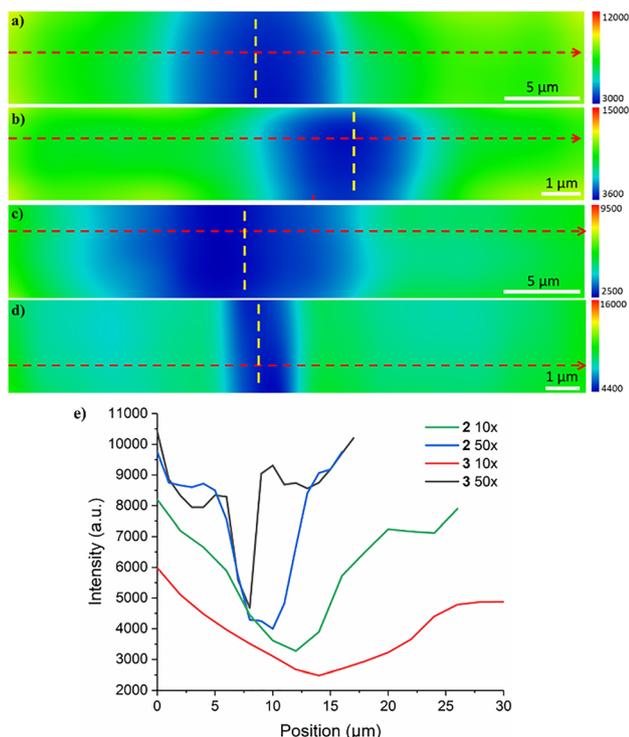
This journal is © the Owner Societies 2025

Phys. Chem. Chem. Phys., 2025, **27**, 22508–22519 | **22515**

Fig. 5 Raman maps of patterns taken at Raman shift of 1226 cm^{-1} and made using (a) the 10× and (b) 50× objectives in a substrate coated with compound **2**, and maps made using (c) the 10× and (d) the 50× objective in a substrate coated with compound **3**. Dashed yellow lines indicate the laser path. (e) The intensity graph taken from the Raman maps along the red dotted lines in Fig. 5(a)−(d). FWHM is used to calculate the 'width' of the trough, with the 'top' of the dip defined as where it levels out.

more quantitatively (Fig. 5(e)). These plots were used to calculate the width of the patterned area by taking the full-width-half-maximum (FWHM) of the dip in the Raman intensity. Based on these figures, the FWHMs of the patterned lines on the samples were approximately 8 μm and 5 μm for compound **2** and for compound **3**, approximately 14 μm and 2 μm for patterns made with 10× and 50× objectives, respectively. For the pyrene compound **3**, we also observe a much shallower 'trough' at 10× magnification, which is partly the reason for the broad linewidth and wider FWHM. As compound **3** has a lower quantum yield than **2** (approximately half),[33] this is somewhat expected, since it is 'smaller' than a full dose, and therefore less of compound **3** would cleave compared to **2**. More importantly, the 10× lines are much wider than the 50× lines for both samples, as could be expected, given the differences in the spot size. Similarly, the photocleavage caused by the 50× objectives created a much 'steeper' dip than the 10× objectives. This strongly implies that the most significant limiting factor for the size of the patterned area is the tightness of the optical exposure and that, subsequently, higher magnifications could produce even smaller features. Another possible method would be to use a photo mask and a simple green light source. Of course, all these methods can be combined for different substrate parts, depending on the desired detail and resolution.

Potential sources of unintended and nonspecific cleavage include light reflection and scattering within the system. As the

underlying substrate is highly reflective silicon, compounds **2** and **3** may be photocleaved by reflected or otherwise scattered light, resulting in wider patterns than desired. Further exploration would require tighter controls over the width of the exposed area, potentially using a photomask. This will be explored further in future work.

Surfaces patterned at lower exposure times resulted in Raman maps (Fig. S8), where the patterns were still discernible even after only 15 s of exposure (at 1.2 mW with the 50× objective). For all three exposures performed using the 50× objective, the lines on the sample coated with compound **3** were 'tighter' than the lines on the sample with compound **2**, consistent with the data for the samples described above. Furthermore, in both cases, the patterned area can be seen (albeit barely) even at 15 s of exposure, which further demonstrates the tunability of this method of surface patterning.

Conclusion

Spatially selective patterning of graphene coated with photocleavable compounds using green light irradiation was demonstrated. The self-assembled layers on pristine graphene were created *via* the π–π adhesion between compounds with naphthalene (**2**) or pyrene (**3**) anchors and the substrate. Photocleavage and its application in light-induced graphene patterning were investigated using Raman spectroscopy, Raman mapping and AFM measurements. A comparison of AFM height sensor data with the dimensions achieved from crystal structures suggests that both compounds form monolayers through face-to-face stacking between aromatic units and graphene. Additionally, their coatings have taller regions, which are either double layers or their different conformations.

AFM measurements of the photocleavable coatings patterned by the green laser revealed a slight increase in height in the pattern created on the layer of compound **2**, and even a smaller increase for compound **3**. However, changes in adhesion in patterned regions were obvious for both compounds. Based on our earlier study, compound **3** exhibits a rate of photocleavage that is almost twice as slow as that of compound **2**, suggesting that photocleavage of compound **2** may also proceed faster on graphene. This may explain the height difference between the patterns.

Photocleavage in a dry state on graphene was confirmed by recording Raman spectra at various time points during the patterning process. The observed changes were similar to our earlier findings, confirming successful photocleavage. The main changes attributed to photocleavage were at 1225 cm^{-1} (Raman peak intensity drop) and 1130–1140 cm^{-1} (Raman peak shift and intensity drop). Additionally, the overall fluorescence, as determined by Raman spectra of both compounds, decreased with increasing exposure time. Raman mapping was performed to further characterize the patterns. It was noted that with a 50× objective, a narrower pattern was achieved with the pyrene anchor (**3**) than with the naphthalene anchor (**2**). Additionally, by adjusting the exposure time or laser spot size,

22516 | *Phys. Chem. Chem. Phys.*, 2025, **27**, 22508–22519

This journal is © the Owner Societies 2025

the degree of photocleavage or pattern size can be controlled. The smallest patterned areas were 2 μm across due to the instrument's resolution limitations. Finer patterns may be available at higher magnifications. The method described here can be applied to PPGs other than BODIPY-based and can be expanded to include covalent functionalization. It also proves that photocleavage is visible by AFM and highly tunable, which boosts its usability in future applications.

The potential application of this method is to guide live nerve cells to grow in a specific direction on the surface of biomaterials, such as implants or biosensors. Amine-functionalized surfaces have been found to attract neuronal cells and enhance their growth.[44–46] Laser-induced formation of amine-functionalized patterns *via* photocleavage of BODIPY-compounds has thus high potential for development of active neuron-guidance techniques.

Author contributions

E. K.: investigation; validation; visualization; writing – original draft; review & editing. E. S: funding acquisition; investigation; formal analysis; visualization; writing – original draft; review & editing; conceptualization. A. E.: investigation; writing – review & editing. A. L.: visualization, writing – review & editing; investigation. M. N.: supervision; writing – review & editing. M. P.: supervision; writing – review & editing.

Conflicts of interest

There are no conflicts to declare.

Data availability

The data supporting this article have been included as part of the supplementary information (SI). Supplementary information is available. See DOI: **https://doi.org/10.1039/d5cp02438b**.

The original files are available upon request from the corresponding author.

Acknowledgements

References

1 V. Georgakilas, M. Otyepka, A. B. Bourlinos, V. Chandra, N. Kim, K. C. Kemp, P. Hobza, R. Zboril and K. S. Kim, Functionalization of Graphene: Covalent and Non-Covalent Approaches, Derivatives and Applications, *Chem. Rev.*, 2012, **112**, 6156–6214.

2 C. Soldano, A. Mahmood and E. Dujardin, Production, properties and potential of graphene, *Carbon*, 2010, **48**, 2127–2150.

3 V. Mishyn, A. Hugo, T. Rodrigues, P. Aspermair, H. Happy, L. Marques, C. Hurot, R. Othmen, V. Bouchiat, R. Boukherroub, W. Knoll and S. Szunerits, The holy grail of pyrene-based surface ligands on the sensitivity of graphene-based field effect transistors, *Sens. Diagn.*, 2022, **1**, 235–244.

4 J. A. Mann and W. R. Dichtel, Improving the Binding Characteristics of Tripodal Compounds on Single Layer Graphene, *ACS Nano*, 2013, **7**, 7193–7199.

5 J. A. Mann, J. Rodríguez-López, H. D. Abruña and W. R. Dichtel, Multivalent Binding Motifs for the Noncovalent Functionalization of Graphene, *J. Am. Chem. Soc.*, 2011, **133**, 17614–17617.

6 D.-W. Lee, T. Kim and M. Lee, An amphiphilic pyrene sheet for selective functionalization of graphene, *Chem. Commun.*, 2011, **47**, 8259–8261.

7 X. Shang, C. H. Park, G. Y. Jung, S. K. Kwak and J. H. Oh, Highly Enantioselective Graphene-Based Chemical Sensors Prepared by Chiral Noncovalent Functionalization, *ACS Appl. Mater. Interfaces*, 2018, **10**, 36194–36201.

8 X. V. Zhen, E. G. Swanson, J. T. Nelson, Y. Zhang, Q. Su, S. J. Koester and P. Bühlmann, Noncovalent Monolayer Modification of Graphene Using Pyrene and Cyclodextrin Receptors for Chemical Sensing, *ACS Appl. Nano Mater.*, 2018, **1**, 2718–2726.

9 A. Silvestri, J. Zayas-Arrabal, M. Vera-Hidalgo, D. D. Silvio, C. Wetzl, M. Martinez-Moro, A. Zurutuza, E. Torres, A. Centeno, A. Maestre, J. M. Gómez, M. Arrastua, M. Elicegui, N. Ontoso, M. Prato, I. Coluzza and A. Criado, Ultrasensitive detection of SARS-CoV-2 spike protein by graphene field-effect transistors, *Nanoscale*, 2023, **15**, 1076–1085.

10 M. Garrido, E. Martínez-Periñán, J. Calbo, L. Rodríguez-Pérez, J. Aragó, E. Lorenzo, E. Ortí, N. Martín and M. Á. Herranz, Supramolecular assembly of pyrene-tetrathiafulvalene hybrids on graphene: structure–property relationships and biosensing activity, *J. Mater. Chem. C*, 2021, **9**, 10944–10951.

11 E. Burzurí, J. O. Island, R. Díaz-Torres, A. Fursina, A. González-Campo, O. Roubeau, S. J. Teat, N. Aliaga-Alcalde, E. Ruiz and H. S. J. van der Zant, Sequential Electron Transport and Vibrational Excitations in an Organic Molecule Coupled to Few-Layer Graphene Electrodes, *ACS Nano*, 2016, **10**, 2521–2527.

12 B. Limburg, J. O. Thomas, G. Holloway, H. Sadeghi, S. Sangtarash, I. C.-Y. Hou, J. Cremers, A. Narita, K. Müllen, C. J. Lambert, G. A. D. Briggs, J. A. Mol and H. L. Anderson, Anchor Groups for Graphene-Porphyrin Single-Molecule Transistors, *Adv. Funct. Mater.*, 2018, **28**, 1803629.

13 J. Cui, L. Chen, Z. Lou, W. Shan and Y. Xiong, Noncovalent functionalization of graphene *via* perylene bisimide-amidoxime for highly efficient capture of uranium, *Sep. Purif. Technol.*, 2025, **361**, 131434.

This journal is © the Owner Societies 2025

Phys. Chem. Chem. Phys., 2025, **27**, 22508–22519 | **22517**

14 M. Hinnemo, J. Zhao, P. Ahlberg, C. Hägglund, V. Djurberg, R. H. Scheicher, S.-L. Zhang and Z.-B. Zhang, On Monolayer Formation of Pyrenebutyric Acid on Graphene, *Langmuir*, 2017, **33**, 3588–3593.

15 Z. Peng, R. Yang, M. A. Kim, L. Li and H. Liu, Influence of O_2, H_2O and airborne hydrocarbons on the properties of selected 2D materials, *RSC Adv.*, 2017, **7**, 27048–27057.

16 A. Lampinen, A. Emelianov, E. See, A. Johansson and M. Pettersson, Effect of two-photon oxidation and calmodulin functionalization on the performance of graphene field-effect transistor biosensors, *RSC Appl. Interfaces*, 2025, **2**, 638–647.

17 J. Koivistoinen, L. Sládková, J. Aumanen, P. Koskinen, K. Roberts, A. Johansson, P. Myllyperkiö and M. Pettersson, From Seeds to Islands: Growth of Oxidized Graphene by Two-Photon Oxidation, *J. Phys. Chem. C*, 2016, **120**, 22330–22341.

18 J. Aumanen, A. Johansson, J. Koivistoinen, P. Myllyperkiö and M. Pettersson, Patterning and tuning of electrical and optical properties of graphene by laser induced two-photon oxidation, *Nanoscale*, 2015, **7**, 2851–2855.

19 A. Johansson, H.-C. Tsai, J. Aumanen, J. Koivistoinen, P. Myllyperkiö, Y.-Z. Hung, M.-C. Chuang, C.-H. Chen, W. Y. Woon and M. Pettersson, Chemical composition of two-photon oxidized graphene, *Carbon*, 2017, **115**, 77–82.

20 K. F. Edelthalhammer, D. Dasler, L. Jurkiewicz, T. Nagel, S. Al-Fogra, F. Hauke and A. Hirsch, Covalent 2D-Engineering of Graphene by Spatially Resolved Laser Writing/Reading/Erasing, *Angew. Chem., Int. Ed.*, 2020, **59**, 23329–23334.

21 A. Piñeiro-García, S. M. Vega-Díaz, F. Tristan, D. Meneses-Rodríguez and V. Semetey, Functionalization and soft photoreduction of graphene oxide triggered by the photo-initiator during thiol-ene radical addition, *FlatChem*, 2022, **33**, 100349.

22 K. Xia, W.-Y. Chiang, C. J. Lockhart de la Rosa, Y. Fujita, S. Toyouchi, H. Yuan, J. Su, H. Masuhara, S. De Gendt, S. De Feyter, J. Hofkens and H. Uji-i, Photo-induced electrodeposition of metallic nanostructures on graphene, *Nanoscale*, 2020, **12**, 11063–11069.

23 Y. Xia, L. Sun, S. Eyley, B. Daelemans, W. Thielemans, J. Seibel and S. De Feyter, Grafting Ink for Direct Writing: Solvation Activated Covalent Functionalization of Graphene, *Adv. Sci.*, 2022, **9**, 2105017.

24 L. Bao, M. Kohring, H. B. Weber, F. Hauke and A. Hirsch, Covalently Doped Graphene Superlattices: Spatially Resolved Supratopic- and Janus-Binding, *J. Am. Chem. Soc.*, 2020, **142**, 16016–16022.

25 M. C. Rodríguez González, A. Leonhardt, H. Stadler, S. Eyley, W. Thielemans, S. De Gendt, K. S. Mali and S. De Feyter, Multicomponent Covalent Chemical Patterning of Graphene, *ACS Nano*, 2021, **15**, 10618–10627.

26 A. Naranjo, M. Garrido, N. Martín Sabanés and E. M. Pérez, Scope and Limitations of Using Microemulsions for the Covalent Patterning of Graphene, *Chem. – Eur. J.*, 2024, **30**, e202303809.

27 T. Wei, S. Al-Fogra, F. Hauke and A. Hirsch, Direct Laser Writing on Graphene with Unprecedented Efficiency of Covalent Two-Dimensional Functionalization, *J. Am. Chem. Soc.*, 2020, **142**, 21926–21931.

28 L. Bao, B. Zhao, M. Assebban, M. Halik, F. Hauke and A. Hirsch, Covalent 2D Patterning, Local Electronic Structure and Polarization Switching of Graphene at the Nanometer Level, *Chem. – Eur. J.*, 2021, **27**, 8709–8713.

29 R. Weinstain, T. Slanina, D. Kand and P. Klán, Visible-to-NIR-Light Activated Release: From Small Molecules to Nanomaterials, *Chem. Rev.*, 2020, **120**, 13135–13272.

30 L. Josa-Culleré and A. Llebaria, In the Search for Photocages Cleavable with Visible Light: An Overview of Recent Advances and Chemical Strategies, *ChemPhotoChem*, 2021, **5**, 296–314.

31 D. Kand, P. Liu, M. X. Navarro, L. J. Fischer, L. Rousso-Noori, D. Friedmann-Morvinski, A. H. Winter, E. W. Miller and R. Weinstain, Water-Soluble BODIPY Photocages with Tunable Cellular Localization, *J. Am. Chem. Soc.*, 2020, **142**, 4970–4974.

32 E. See, E. Korhonen, M. Nissinen and M. Pettersson, Non-covalent attachment of BODIPY-caged amines to graphene and their localized photocleavage, *New J. Chem.*, 2024, **48**, 21–25.

33 E. Korhonen, T. Kumpulainen, M. Pamula, A. Valkonen, E. See, M. Pettersson and M. Nissinen, Photocleavage and Photophysical Properties of Amine Releasing BODIPY Derivatives, *Chem. – Eur. J.*, 2025, **31**, e202500530.

34 P. Shrestha, D. Kand, R. Weinstain and A. H. Winter, *meso*-Methyl BODIPY Photocages: Mechanisms, Photochemical Properties, and Applications, *J. Am. Chem. Soc.*, 2023, **145**, 17497–17514.

35 S. M. Kozlov, F. Viñes and A. Görling, On the interaction of polycyclic aromatic compounds with graphene, *Carbon*, 2012, **50**, 2482–2492.

36 A. Z. AlZahrani, First-principles study on the structural and electronic properties of graphene upon benzene and naphthalene adsorption, *Appl. Surf. Sci.*, 2010, **257**, 807–810.

37 A. Karton, π–π interactions between benzene and graphene by means of large-scale DFT-D4 calculations, *Chem. Phys.*, 2022, **561**, 111606.

38 S. D. Chakarova-Käck, E. Schröder, B. I. Lundqvist and D. C. Langreth, Application of van der Waals Density Functional to an Extended System: Adsorption of Benzene and Naphthalene on Graphite, *Phys. Rev. Lett.*, 2006, **96**, 146107.

39 M. Cao, A. Fu, Z. Wang, J. Liu, N. Kong, X. Zong, H. Liu and J. J. Gooding, Electrochemical and Theoretical Study of π–π Stacking Interactions between Graphitic Surfaces and Pyrene Derivatives, *J. Phys. Chem. C*, 2014, **118**, 2650–2659.

40 S. Mula, A. K. Ray, M. Banerjee, T. Chaudhuri, K. Dasgupta and S. Chattopadhyay, Design and Development of a New Pyrromethene Dye with Improved Photostability and Lasing Efficiency: Theoretical Rationalization of Photophysical and Photochemical Properties, *J. Org. Chem.*, 2008, **73**, 2146–2154.

41 J. S. Sandoval, Q. Gong, L. Jiao and D. W. McCamant, Stimulated Resonance Raman and Excited-State Dynamics in an Excitonically Coupled Bodipy Dimer: A Test for

22518 | *Phys. Chem. Chem. Phys.*, 2025, **27**, 22508–22519

This journal is © the Owner Societies 2025

TD-DFT and the Polarizable Continuum Model, *J. Phys. Chem. A*, 2023, **127**, 7156–7167.

42 D.-Y. Wu, X.-M. Liu, Y.-F. Huang, B. Ren, X. Xu and Z.-Q. Tian, Surface Catalytic Coupling Reaction of *p*-Mercaptoaniline Linking to Silver Nanostructures Responsible for Abnormal SERS Enhancement: A DFT Study, *J. Phys. Chem. C*, 2009, **113**, 18212–18222.

43 J. E. Lee, G. Ahn, J. Shim, Y. S. Lee and S. Ryu, Optical separation of mechanical strain from charge doping in graphene, *Nat. Commun.*, 2012, **3**, 1024.

44 Y.-J. Ren, H. Zhang, H. Huang, X.-M. Wang, Z.-Y. Zhou, F.-Z. Cui and Y.-H. An, *In vitro* behavior of neural stem cells in response to different chemical functional groups, *Biomaterials*, 2009, **30**, 1036–1044.

45 A. P. Hopper, J. M. Dugan, A. A. Gill, O. J. L. Fox, P. W. May, J. W. Haycock and F. Claeyssens, Amine functionalized nanodiamond promotes cellular adhesion, proliferation and neurite outgrowth, *Biomed. Mater.*, 2014, **9**, 045009.

46 C. S. Taylor, R. Chen, R. D' Sa, J. A. Hunt, J. M. Curran and J. W. Haycock, Cost effective optimised synthetic surface modification strategies for enhanced control of neuronal cell differentiation and supporting neuronal and Schwann cell viability, *J. Biomed. Mater. Res.*, 2021, **109**, 1713–1723.

This journal is © the Owner Societies 2025

Phys. Chem. Chem. Phys., 2025, **27**, 22508–22519 | **22519**